Optik - International Journal for Light and Electron Optics 243 (2021) 167335

Contents lists available at ScienceDirect

Optik

journal homepage: www.elsevier.com/locate/ijleo

Research on-orbit temperature variation stability of the positioning accuracy of maintenance interface

Yanyan Wen [a,b,*], Libao Yang [c], Zhen Shi [c], Songhang Wu [c], Zhirong Lu [c], Lixia Shi [a,b,*]

[a] School of Optoelectronic Engineering, Changchun University of Science and Technology, Changchun 130022, China
[b] National Demonstration Center for Experimental Optoelectronic Engineering Education, School of Optoelectronic Engineering, Changchun University of Science and Technology, Changchun 130022, China
[c] Changchun Institute of Optics, Fine Mechanics and Physics, Chinese Academy of Sciences, Changchun 130033, China

ARTICLE INFO

Keywords:
Space optical telescope
On-orbit maintenance
Interface mechanism
Heat stress release
Positioning accuracy

ABSTRACT

The space telescope is running, which is influenced by the rapid temperature difference. The paper analyzes the stability of the space environment of the on-orbit maintenance interface. The influence of temperature changes on the positioning of the interface mechanism is studied. Based on the 3-2-1 kinematic positioning principle, a mathematical model is established, and the mathematical expression of the on-orbit positioning accuracy of the back-end module between the temperature change and the interface layout point is deduced, and the variation quantity and the displacement variation of the angle of the center point are derived. The results show that when the line of AB points coincides with the positioning axis of B point, the rotation angle of the back-end module in the plane composed of A, B, C three points is the smallest. Through the relationship between the four independent variables λ, μ, η, t and the change of the central point ΔE, it is concluded that when A, B, C three-point layout is obtained, to make the back-end module have the highest stability, the order of variable design should be η, t, λ and μ. The suspension wire system was used to build a ground microgravity simulation test rig. The gravity unloading and thermal stress tests were carried out by the balancing mass method. The thermal stress test results prove that the interface can realize kinematics positioning and complete the on-orbit thermal stress release.

1. Introduction

When the space telescope is running, the back-end module interface mainly supports the function of positioning. To ensure the regular operation of the space telescope, the stability of the interface must be higher. The form of bad environment is varied, including the vacuum environment effect, the atmosphere is reduced, the microgravity environment, the gravity disappearance of the ground, the vacuum discharge effect, the weak magnetic field effect, the plasma environment effect, the space radiation ultraviolet effect and so on. In many environmental factors, severe temperature changes are the most brutal conditions. This interface is a positioning mode designed according to the kinematics principle. When the temperature changes are intense, the interface will release the heat stress and

* Corresponding authors at: School of Optoelectronic Engineering, Changchun University of Science and Technology, Changchun 130022, China.
E-mail addresses: w15628841185@163.com (Y. Wen), yanglibao228@163.com (L. Yang), shizhen199@163.com (Z. Shi), wusonghang17@mails.ucas.ac.cn (S. Wu), luzhirong18@mails.ucas.edu.cn (Z. Lu), custslx@cust.edu.cn (L. Shi).

https://doi.org/10.1016/j.ijleo.2021.167335
Received 21 April 2021; Accepted 28 May 2021
Available online 2 June 2021

reduce the stress concentration, making small changes in the module's location. To maintain the high point accuracy of the space telescope, the stability of the back-end module is reasonable.

At present, on-orbit replacement technology has been fully expanded , such as the Skylab [1–5], the Solar Maximum Mission (SMM) [6–8], the Hubble Space Telescope(HST) [9–18], the Engineering Test Satellite No.7(ETS-VII) [19–22], the James Webb Space Telescope (JWST) [23–26] et al. The biggest obstacle for spacecraft in the space environment is the change of space temperature. In the James Webb Space Telescope (JWST), both the Fine Guidance Sensor (FGS) and the Integrated Science Instrument Module (ISIM) [27, 28] are connected to the primary system via quasi-kinematic coupling, which restrains the transfer of mechanical and thermal deformations between the main structure and the ISIM. Wang et al. studied the influence of temperature on the primary mirror type [29]. Yang et al. studied the effect of temperature on the concentration [30]. Liu et al. studied the influence of temperature on the measurement error of the star sensor [31]. Yang et al. studied the effect of temperature gradient on the stability tolerance of reflectors [32]. In the on-orbit operation of the space telescope, there is a large difference in the layout of the mounting interface between different instruments and the temperature between the optical system and the mounting platform [33]. The interface layout and temperature may stress the optical system. New ways are needed to reduce the differences and eliminate the stress.

Based on the 3-2-1 kinematics principle, and the mathematical expression of the accuracy of the back-end module is derived from the temperature change and the interface layout, and the corresponding angle of the back-end module is the minimum in the flat angle of the A, B, C. The temperature change formula of the layout point allocation distribution provides a reference price for further streamlining the layout and design of the interface.

2. Study on temperature stability of interface mechanism

In the space environment, the spacecraft will face complex space environment changes, especially violent temperature changes. The interface mechanism should ensure the imaging stability and accuracy of the space telescope in orbit for a long time. It must have good adaptability to the space environment of hot and cold. The purpose of installing the interface mechanism is to ensure the speedy replacement of the optical load on the rail and the correct installation of the back-end module and the main optical machine, and the location layout should be considered emphatically [34,35]. This interface adopts 321 kinematic positioning modes. As shown in Fig. 1, there are three support points, which are defined as A, B, C. The support positioning interface A limits the movement of the back-end module in three directions in space and releases three rotational degrees of freedom. The support location interface B restricts y-direction and z-direction to the back-end module and releases four other degrees of freedom. The support positioning interface C restricts the back-end module z-direction and releases the other five degrees of freedom and the A, B, C three-point function to realize the static support of the back-end module. As showing in Fig. 2, when the temperature changes, the whole back-end module takes a point at the center to expand or shrink. The B point moves along the y-axis, the C point moves in the x-y plane, and the whole back-end module is uniformly deformed, so it will not produce thermal stress inside, thus avoiding the harm caused by thermal stress.

2.1. Mathematical model of temperature change of interface mechanism

A plane consists of three positioning points of the maintainable back-end module, and the A, B, C three-point plane should be parallel to the disassembly direction of the module. A, B two points are located on both sides of the maintainability back-end module. The projection of the plane is composed of A, B, C three points in the plane is shown in Fig. 3. Establish the coordinate system as shown in Fig. 3, and take the rectangle surrounded by A, B, C three points as the reference boundary. According to the analysis of A, B, C three-point constrained degrees of freedom, when the temperature changes, the A point limits the translational degrees of freedom in three directions, so there will be no translational motion. The A point releases three rotational degrees of freedom at the same time. Therefore, it produces its specific rotation at the A point. The B point releases the axial translation degree of freedom, so the B point will have the physical change of thermal expansion and contraction along the x-direction of the axis, that is, the coordinate system. The C point will also change in the x-y direction of translation degree of freedom. The whole repairable back-end module will produce

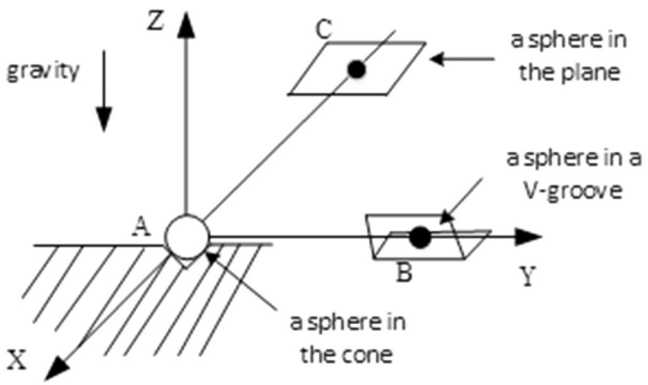

Fig. 1. Kinematically positioning method.

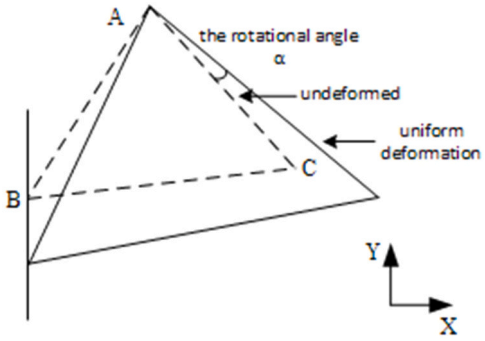

Fig. 2. Moving trend of structure.

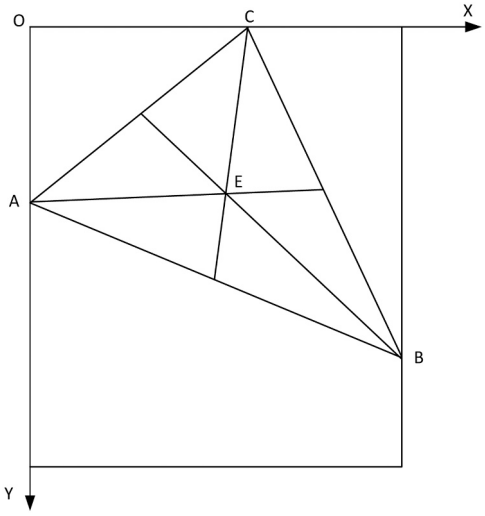

Fig. 3. A, B, C three-point spatial layout.

rotation deformation around the A point, but it will not make translation motion in the z-direction. The thermal stress caused by the temperature change of the space environment is converted by the release of the degree of freedom, which will not produce the thermal stress concentration on the structure and avoid the failure of the interface structure. Therefore, only the focal plane is required to be parallel to the A, B, C connection plane, which can ensure the theoretical basis of stable imaging at all-time in the environment of temperature change.

The space layout of the A, B, C three-point before temperature changes is shown in Fig. 3: The spatial coordinates of A are (A_x, A_y, A_z), The spatial coordinates of B are (B_x, B_y, B_z), The spatial coordinates of C are (C_x, C_y, C_z). The rectangle length of ABC is L and τL. L is the length of the rectangle in the x-direction of the coordinate system and τL indicates the length of the rectangle in the y-direction of the coordinate system.

The center of the triangle ABC is represented by E:

$$E = \frac{A + B + C}{3} \tag{1}$$

The spatial coordinates of A are (E_x, E_y, E_z), the space coordinates of A, B, C three points are shown in Table 1. And the λ, μ and η is the coefficients of each point in the coordinates before that, and the value of λ and μ are (0, ∞), and the value of η is (0,1).

Table 1
Spatial coordinates of three points.

Axis	A	B	C	E
X	0	L	ηL	$L(1+\eta)/3$
Y	λL	μL	0	$L(\lambda+\mu)/3$
Z	0	0	0	0

When the temperature changes, the B point moves along the axial direction, from the original position to the B1 point after the temperature rise. The C point changes from the initial position to the C_1 point after the temperature rise, and the A point remains unchanged. The center point E becomes the E_1 point after the temperature rise. The projection of A point on the other side of the rectangle is shown in D, as shown in Fig. 4. The angle α is the angle between line AB and line AB_1, which represents the angle of the whole module, and the angle β is the angle of the line AC and the line AD. Based on the theory of temperature change:

$$\begin{cases} L_{AB1} = a\Delta T L_{AB} \\ L_{AC1} = a\Delta T L_{AC} \\ E = \dfrac{A+B+C}{3} \\ E1 = \dfrac{A+B1+C1}{3} \\ L^2{}_{AB1} = (L_{AD} + L_{BB1})^2 + L^2{}_{DB} \\ \Delta E = E1 - E \end{cases} \tag{2}$$

$$L_{BB1} = L\sigma \tag{3}$$

$$\alpha = \arctan\left(\frac{(\mu-\lambda)\sigma}{1+\sigma+(\mu-\lambda)^2}\right) \tag{4}$$

$$\sigma = \sqrt{\left(2a\Delta T + (a\Delta T)^2\right)(\lambda-\mu)^2 + (1+(a\Delta T))^2} - 1 \tag{5}$$

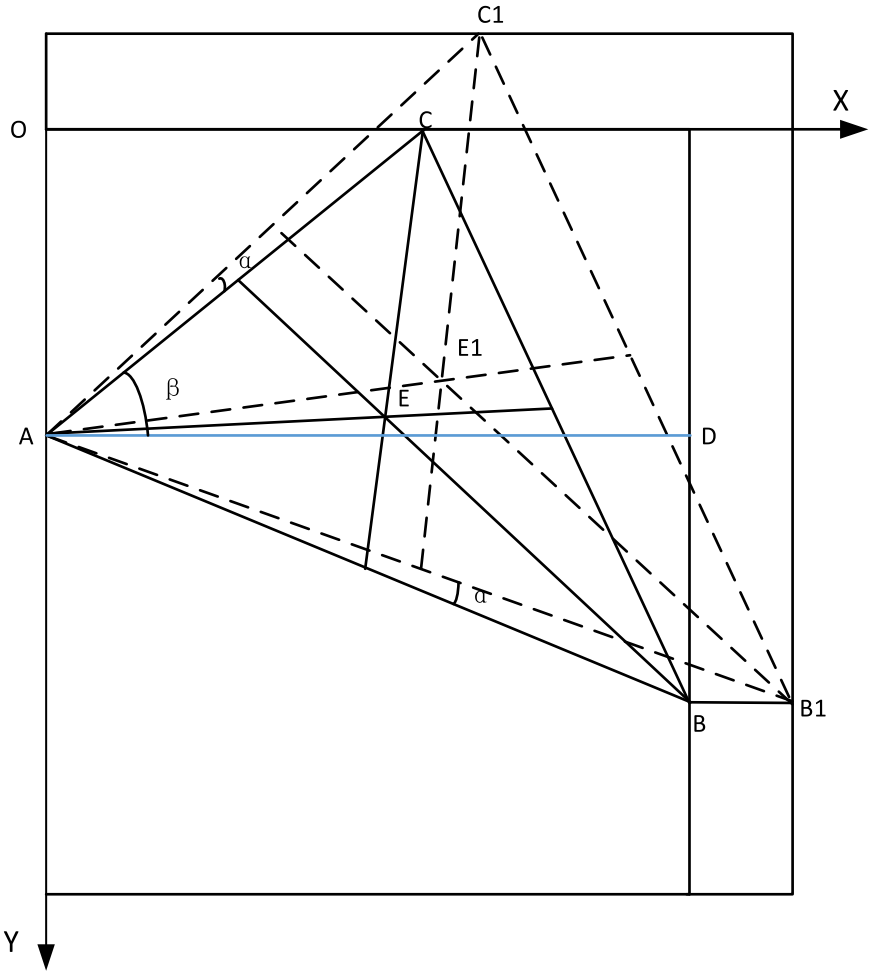

Fig. 4. A, B, C three-point temperature change process diagram.

In the formula (2), a indicates the overall thermal expansion coefficient of the back-end module. ΔT represents the rising temperature. L_{AB} defines the length between A and B. L_{AB1} defines the length between A and B_1. L_{AC} represents the length between A and C. L_{AC1} describes the length between A and C_1. L_{BB1} describes the length between B and B_1. To be able to indicate the location of the posterior terminal module after the temperature rise, the change in the central point E of the triangle ABC is expressed by the various points of Table 1, which is solved by:

2.2. Effect of temperature variation on positioning accuracy

As shown in Table 2, the change of central point E in the x-direction is represented by ΔE_x, and the change of central point E in the y-direction is represented by ΔE_y.

$$\Delta E_x = \frac{L\left[\sigma - \eta + \left(1 + a \triangle T\right)\sqrt{\lambda^2 + \eta^2}\cos\left(\arctan\left(\frac{\eta\sigma(\mu-\lambda)+\lambda\left[1+\sigma+(\mu-\lambda)^2\right]}{\eta[1+\sigma+(\mu-\lambda)^2]-\lambda\sigma(\mu-\lambda)}\right)\right)\right]}{3} \tag{6}$$

$$\Delta E_y = \frac{L\left[\left(1 + a \triangle T\right)\sqrt{\lambda^2 + \eta^2}\sin\left(\arctan\left(\frac{\eta\sigma(\mu-\lambda)+\lambda\left[1+\sigma+(\mu-\lambda)^2\right]}{\eta[1+\sigma+(\mu-\lambda)^2]-\lambda\sigma(\mu-\lambda)}\right)\right) - \lambda\right]}{3} \tag{7}$$

The distance before and after the change of center point E is denoted by ΔE;

$$\Delta E = \left((\Delta E_x)^2 + (\Delta E_y)^2\right)^{0.5} \tag{8}$$

Firstly, the rotation angle α is numerically analyzed. According to the above formula, the change of angle α is only related to the values of λ and μ among the three coordinate coefficients and has nothing to do with the values of η. (thermal expansion coefficient is 0.00001, ΔT is 20). According to Fig. 5, the sensitivity of λ to angle α is the same as that of μ to angle α. The values of λ and μ are (0, 2), and we can see that the angle α varies from 0 to plus or minus 80 s. When $\lambda < \mu$, the back-end module rotates clockwise about the z-axis around point A, and when $\lambda > \mu$, the back-end module rotates counterclockwise about the z-axis around point A. When the fixed relation $\lambda = \mu$, the change of angle α is 0, the temperature of point B changes along the line direction of AB, and that of point C changes along the direction of AC, the changing trend is shown in Fig. 6.

The influence of temperature change on the back-end module is measured by the change amount of the center of the triangle surrounded by three points A, B, C. When angle α is 0, the change of central point E in the x-y direction is simplified as formula (9) and (10).

$$\Delta E_x = \frac{L\left[\sigma - \eta + \left(1 + a \triangle T\right)\sqrt{\lambda^2 + \eta^2}\cos\left(\arctan\left(\frac{\lambda}{\eta}\right)\right)\right]}{3} \tag{9}$$

$$\Delta E_y = \frac{L\left[\left(1 + a \triangle T\right)\sqrt{\lambda^2 + \eta^2}\sin\left(\arctan\left(\frac{\lambda}{\eta}\right)\right) - \lambda\right]}{3} \tag{10}$$

The change in the central point E in the x-y direction is defined by the ΔE_x and ΔE_y, and the overall change in the x-y surface is expressed by the ΔE. The influence trend of λ and t on them is shown in Fig. 7, and the value of λ is (0–2), and the value of t is (0–30), and the constant quantity of η is 0.5. when the $\lambda = \mu$, the $\Delta E_x, \Delta E_y$ and ΔE increases the approximation linearly with the temperature growth; the $\Delta E_x, \Delta E_y$ and ΔE increases the nonlinearly with the λ values increase; Of them, ΔE_y and ΔE are more sensitive, and the insensitivity of ΔE_x.

The influence trend of λ and η on the $\Delta E_x, \Delta E_y$ and ΔE is shown in Fig. 8, and the value of λ is (0, 2), the value of η is (0–1), and the constant quantity of t is evaluated by 30 °C. When $\lambda = \mu$, the increase of ΔE_x, ΔE_y and ΔE with the rise of η is nonlinear. So when

Table 2
Spatial coordinates of three points after temperature change.

Axis	B1	C1
X	(σ+1)L	$(1 + a \triangle T)L\sqrt{\lambda^2 + \eta^2}\cos(\arctan(\frac{\eta\sigma(\mu-\lambda)+\lambda[1+\sigma+(\mu-\lambda)^2]}{\eta[1+\sigma+(\mu-\lambda)^2]-\lambda\sigma(\mu-\lambda)}))$
Y	μL	$((1 + a \triangle T)\sqrt{\lambda^2 + \eta^2}\sin(\arctan(\frac{\eta\sigma(\mu-\lambda)+\lambda[1+\sigma+(\mu-\lambda)^2]}{\eta[1+\sigma+(\mu-\lambda)^2]-\lambda\sigma(\mu-\lambda)})) - \lambda)L$
Z	0	0
Axis	E	E1
X	L(1+η)/3	$\frac{L[\sigma+1+(1+a \triangle T)\sqrt{\lambda^2+\eta^2}\cos(\arctan(\frac{\eta\sigma(\mu-\lambda)+\lambda[1+\sigma+(\mu-\lambda)^2]}{\eta[1+\sigma+(\mu-\lambda)^2]-\lambda\sigma(\mu-\lambda)}))]}{3}$
Y	L(λ+μ)/3	$\frac{L[\mu+(1+a \triangle T)\sqrt{\lambda^2+\eta^2}\sin(\arctan(\frac{\eta\sigma(\mu-\lambda)+\lambda[1+\sigma+(\mu-\lambda)^2]}{\eta[1+\sigma+(\mu-\lambda)^2]-\lambda\sigma(\mu-\lambda)}))]}{3}$
Z	0	0

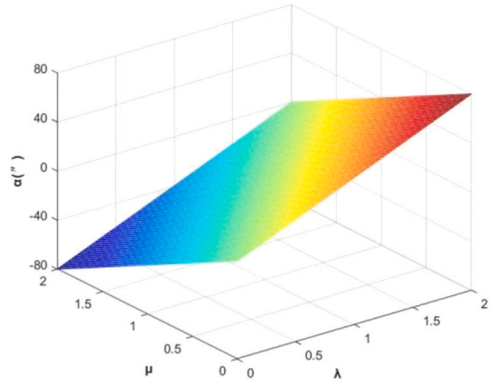

Fig. 5. The influence of variables λ and μ on angle α.

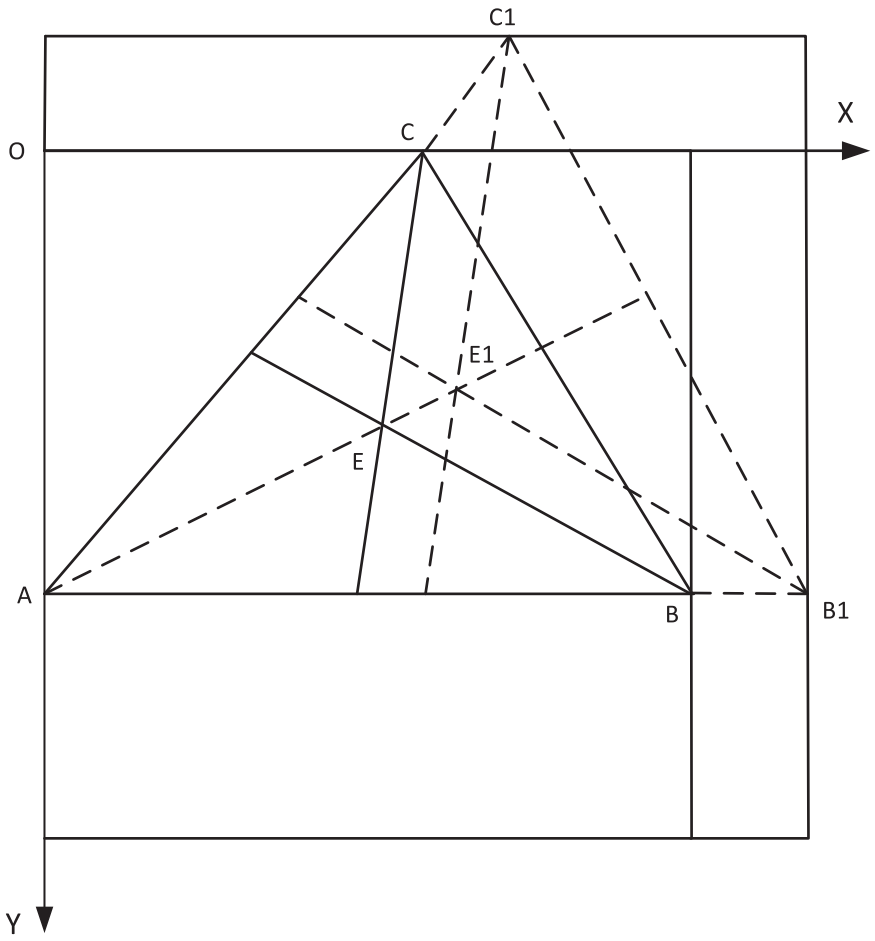

Fig. 6. A, B, C three-point temperature change process diagram ($\lambda = \mu$).

the three points of the layout meet the overall angle of the x-y plane is 0, the value of λ and η should be smaller when satisfying the reasonable overall layout and the load so that the center point E can maintain high stability in the same temperature changing environment.

When $\lambda \neq \mu$, the angle α is not 0. Without considering the change of E in the single square, the change in the overall change of ΔE is studied, and study the changing relationship between the ΔE and four independent variables. To maintain the high stability of the back-end module in the temperature of the space environment, the change in the ΔE change must be small. The influence of four variables and ΔE are shown in Fig. 9. The red dots in the figure indicate the relationship between the changing trend of the minimum value of the

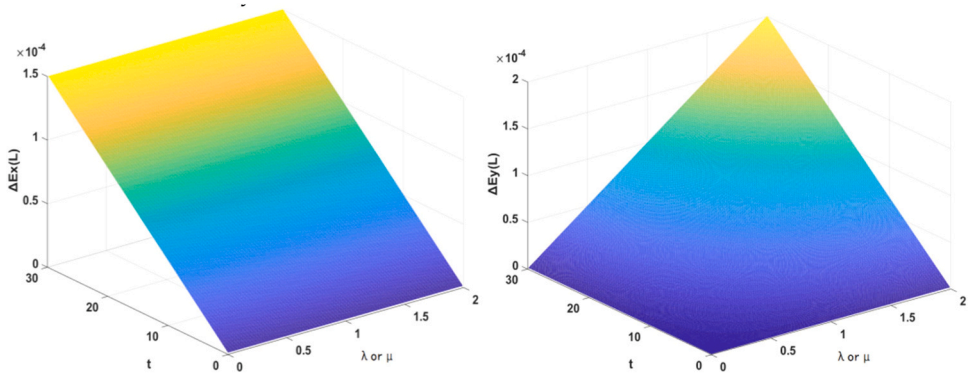

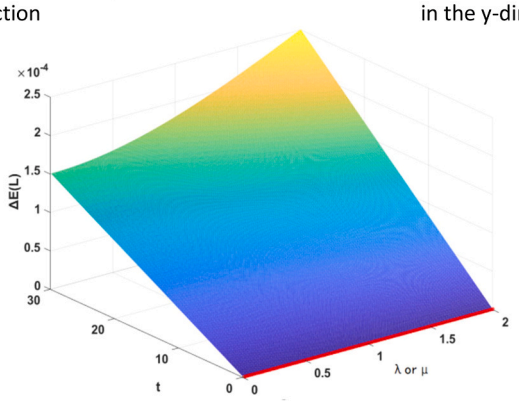

Fig. 7. The influence of variables λ and t on positioning accuracy ($\lambda = \mu$).

dependent variable and the independent variable within the range of independent variable change. The variation range and fixed value of independent variables are shown in Table 3.

From Fig. 9, ΔE increases linearly with the increase of η, and when η is combined with its three variables, η is the dominant factor. All of the minimum values of ΔE are at the most minor point of η, which is not changed by the change of the other three variables. So the location layout of A, B, C's three-point distribution is first to consider the appropriate installation location of η, and η to try not to be too large, it better to control 0.5 of the entire back-end module and then consider three other variables.

The effect of t on the temperature stability of the entire back-end module space: when t and η are combined, it is weak in η, but when combined with μ and λ, the minimum value appears at the minimum point of t, and the effect of t on the whole back-end module space stability is significantly stronger than μ and λ. The stability of the back-end module decreases with the increase of t and presents an approximately linear relationship. In the case of conditions, try to apply temperature control measures to the interface and its overall rear back-end module, aiming to reduce the stability of the temperature.

Among them, the effects of λ and μ on the complementary effects of the entire back-end module are the weakest, so the layout of λ and μ should be considered in the final consideration. But the overall stability of λ and μ is not a single change trend, and the change ΔE in the back-end module center is increased by the increase of λ and μ, and the change in λ in the same change is faster than the change in μ. Fig. 9 shows that when the value of η and t is determined, the maximum stability of the module is that the maximum, λ and μ must be linear, the different λ and μ determine the different linear proportional factors. From Fig. 9, when η values 0.5, t to 30, the rear end module wants to make the maximum stability, making the $\mu = 0.65\lambda$.

3. Verifying the stress release on-orbit

3.1. The test process of the stress release on-orbit

When the repairable back-end module on-orbit, the biggest problem is whether it can adapt to the change of high and low temperature in space to ensure higher image quality. The A, B, C three-point interface processing the test tooling, and the theoretical formula derived in the second section is verified. The A, B, C three-point interface and the test back-end module must be in the same installation plane during the test. The λ value of A, B two points installed in the same plane is equal to the η value to verify the displacement variation of B, C two points.

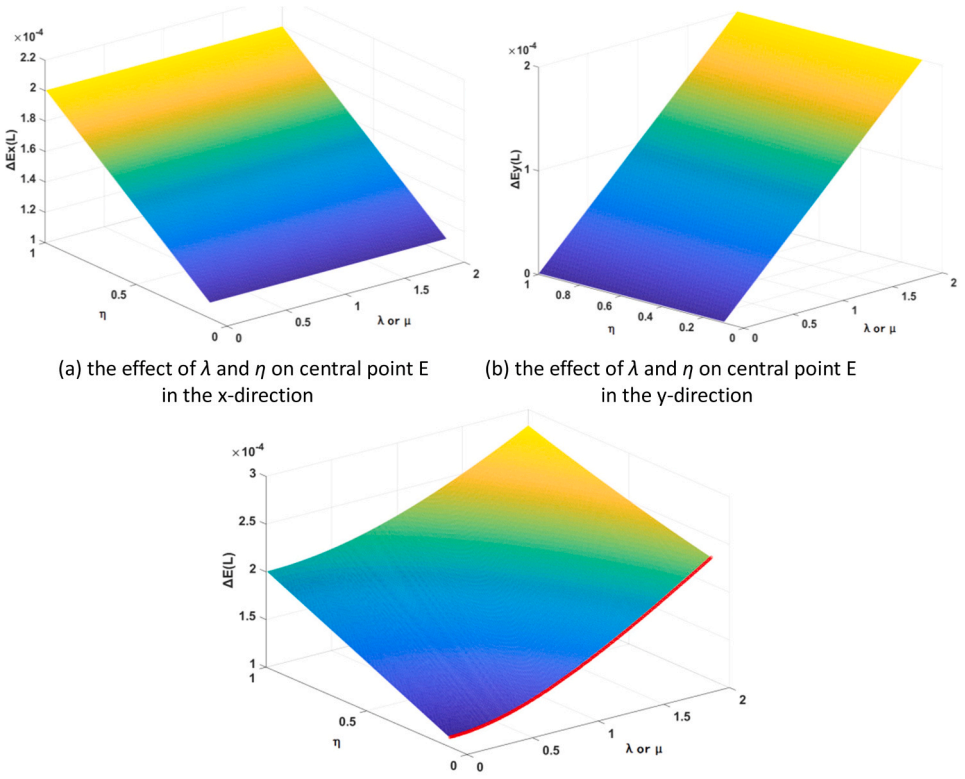

Fig. 8. The influence of variables λ and η on positioning accuracy ($\lambda = \mu$).

In this experiment, the back-end test module is unloaded by the suspension wire system. First, the whole back-end module is unloaded and installed under the action of the suspension device. After installation, the real mass of the movable component of the whole back-end test module is measured by the suspension device. The fixed pulley is installed on the beam hanger, the wire passes through the fixed pulley, one end is connected with the optical back-end test load module, and one end is hoisted with the lead block to realize the gravity unloading of the optical load module. The whole process must make the test load module without resistance follower under small external force before the subsequent work can be carried out.

Before the experiment, the laser tracking device's global coordinate system is used to establish the coordinate system to the coordinate system and compensate the coordinates of the target. Compensation consists of two parts in the optical axis, and part of the radius of the target is half the thickness of the test, and the non-optical axis is only for the radius of the target. In the laboratory environment of normal pressure and temperature, the test of the light spot stability of the two instruments is verified. One is a laser tracking device used in testing verification of thermal stress release and repeatability accuracy. The other instrument is the auto-collimator instrument, which will be used to validate repeated positioning accuracy. The spot points of the laser tracker were collected for 30 min continuously, and the spatial coordinates of the target ball were calculated. The standard deviation of the target ball in the x, y, and z-directions were 0.48 μm, 0.39 μm, 0.40 μm. The light spots of the two auto-collimator spots of the test were collected for 30 min, and the angle of the x, y and z-directions of the was 0.0055 s, 0.0065 s and 0.0058 s. The light spot of the measuring instrument has high stability in 30 min, and the requirement of the precision measurement of the system is achieved, and the effect of the spot drift is negligible.

3.1.1. Test planning

The heat stress release test is adopted by the aluminum alloy (LC9). It is very sensitive to heat deformation and can better verify the heat effect and the best choice for the module installation board. Its thermal expansion coefficient a is 2.36 $e^{-5/°C}$. As shown in Fig. 10, paste eight pieces of the same heating plate on the table surface of the test module, make the heating film cover the entire mounting board, and only set up the location of the target ball on the mounting plate. The eight heating pieces must be evenly distributed to achieve continuous heating and stable temperature. The specifications of the heating chip are made of silicon rubber heating, which has the characteristics of heating fast, temperature uniformity, high heat efficiency, high strength, convenient use, long safe life, and easy aging. The rated voltage is a variable alternating current of 1-66v. The maximum heating temperature can reach 75%. Two heating power sources are used to heat the test module in the test environment. The installation interface of the module and interface is reinforced with insulation and reduces the effect of the interface's deformation on the test results. As shown in Fig. 11, two dial indicators are placed separately in both the interface B and C. The dial indicator 1 measures the position of the B point axis, and the

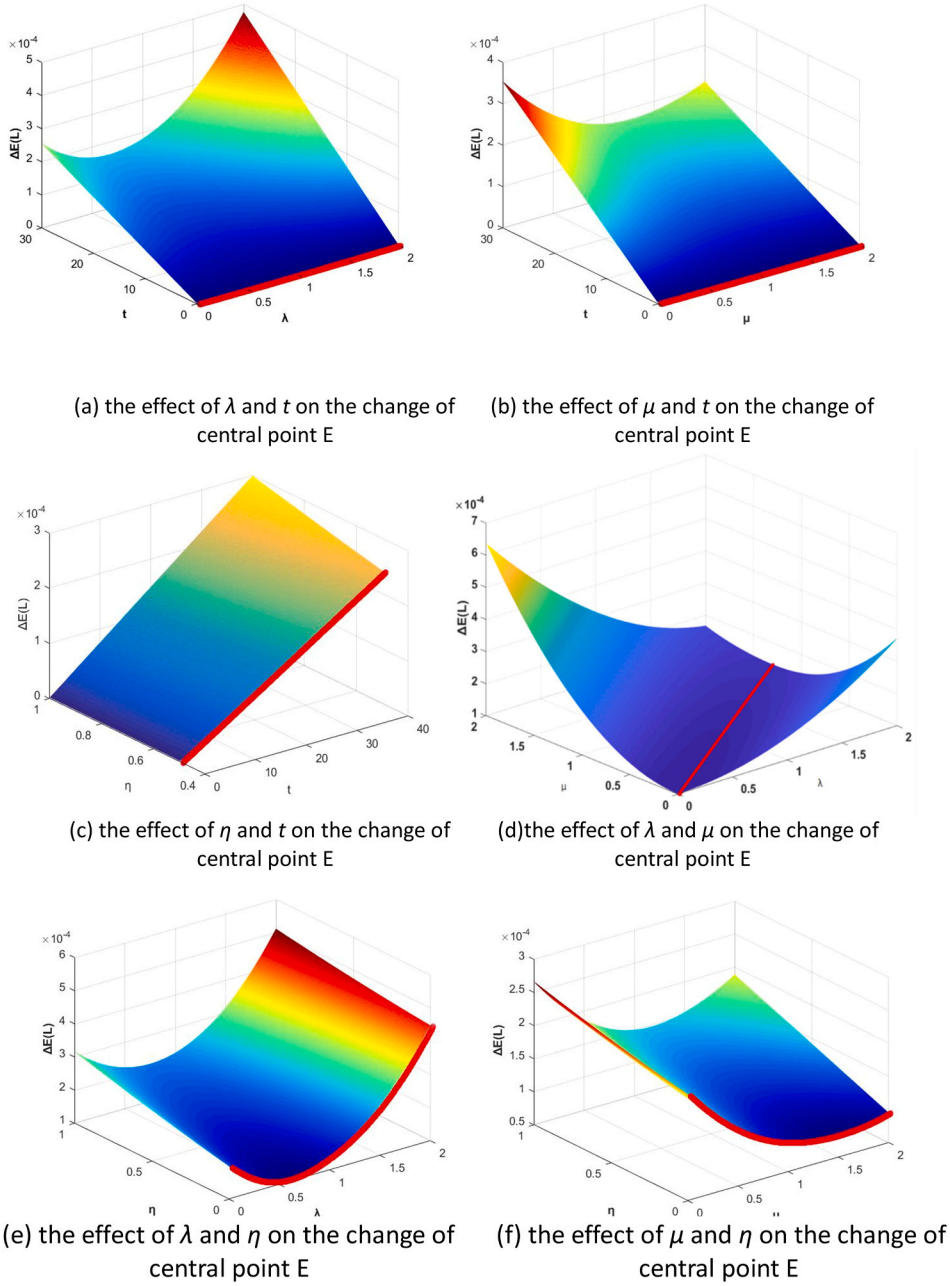

Fig. 9. The influence of variables on positioning accuracy.

Table 3
Spatial coordinates of three points after temperature change.

Independent variable	λ	μ	η	t
Fixed value	1	1	0.5	30
Variable value	(0–2)	(0–2)	(0–1)	(0–30)

measurement points are changing in the direction of the x-axis. The dial indicator 2 measuring the amount of change in support of B. The variation of the C point axis is measured by dial indicator 3, which is the change in the direction of the y-direction and the change in the measurement of C points in dial indicator 4. In the table surface of the test module, three targets are placed on the surface of the test module, and the target ball is placed on the installation table of the test module. The laser tracking instrument measures the space

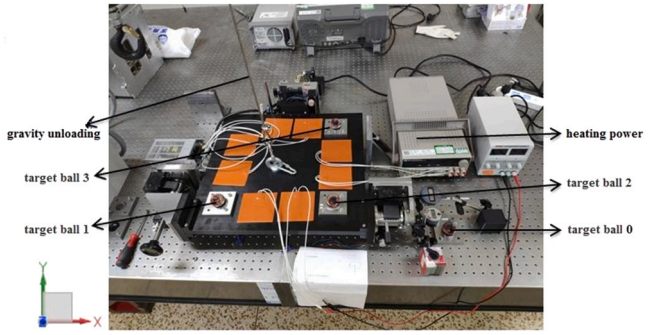

Fig. 10. Thermal experiment science.

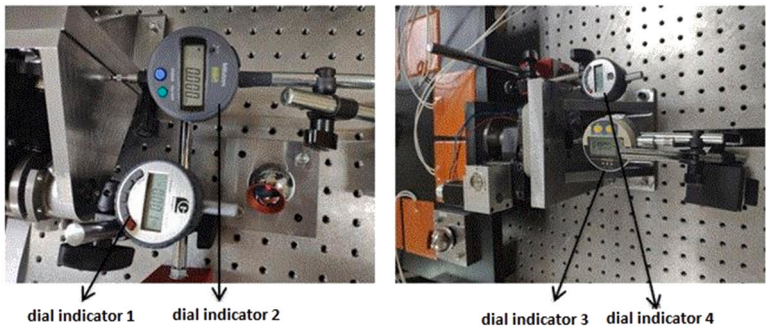

(a) The layout of the dial indicator at point B (b)The layout of the dial indicator at point C

Fig. 11. Layout of dial indicator.

coordinates changes. The temperature of the experiment was 22℃. The module was heated at a constant temperature, and the variation of each dial meter was recorded. The average value of the dial meter 1-4 at each temperature was obtained through multiple measurements.

Before testing, complete the installation of the test module according to the layout of the work in the plane. The test installation table is the benchmark. The dial indicator and the laser tracking instrument are the test measuring device, ensuring the installation plane and the entire installation table are located at the same height. And gently turn the B point and feel comfortable and undisturbed to carry out the heat stress release test. The initial temperature of the test environment is 20 °C, and from the increase to 25 °C, the measurement results of the two instruments are recorded by the 3 °C. The average number of measures the following measurement data.

3.2. Analysis of the experimental results of the stress release on-orbit

In Fig. 10, there are four target balls, target ball 0, which is measured by several times, and the Table 4 is the recorded value of the test results. The Table 4 show that the target ball 0 is not changed. The table is not affected by the external environment, and the benchmark reliability of the whole heat test is high. The target ball 1 is near the A point of the entire test module, so it is stable in temperature change. Target ball 2 near the test module point B, thermal stress will be released at point B along the x-direction in the figure after temperature rise occurs. The whole module will expand and contract linearly at the fixed point of point A in the x-direction. Therefore, the x coordinate of target ball 2 will increase linearly with the change of temperature. The data in the figure is consistent with the theory. The target ball 3 is close to the y-axis of point C, and the x-coordinate of target ball 2 is the same. Since there is no constraint on the x-y direction of point C, after the temperature rises, the linear release of point C will occur in the plane's x-y direction. The variation trend of target ball 3 was also observed, which was consistent with the theoretical deduction.

The error size of the theoretical formula and test value is verified by the measurement data of the dial indicator. In a large number of repeated heating, the variation of the dial indicator 2 and the dial indicator 4 shows between 0 and 0.001. The support surface of the installation interface is not changed, which can ensure the installation stability of the back-end module and the main optical machine. Table 5 is the recorded value of dial indicator 1 and dial indicator 3.

According to the 3-2-1 kinematic positioning principle, the module is not moving at A point, and the BC point will be released in the direction of the line of the A point. The change in the displacement of two points BC is expressed as the following formula:

$$\Delta L_{BX} = \left(\sqrt{\left(2a\Delta T + (a\Delta T)^2\right)(\lambda-\mu)^2 + (1+(a\Delta T))^2} - 1\right)L \tag{11}$$

Table 4
Experimental data of laser tracker (thermal stress release test).

The temperature after heating	Average temperature variation of target ball 0 (mm)			Average temperature variation of target ball 1 (mm)		
axis	x0	y0	z0	x1	y1	z1
25	0.001	-0.001	0.001	0.003	-0.001	0.001
28	0.002	0.001	0.000	0.004	0.002	0.001
31	0.002	0.002	0.001	0.014	0.002	0.001
34	0.001	0.001	-0.002	0.017	0.002	0.003
37	0.002	0.000	0.001	0.023	0.001	0.004
40	0.001	0.002	0.000	0.022	0.002	0.003
43	-0.001	0.002	-0.001	0.031	0.004	0.003
The temperature after heating	Average temperature variation of target ball 2(mm)			Average temperature variation of target ball 3(mm)		
axis	x2	y2	z2	x3	y3	z3
25	0.022	0.002	-0.001	0.027	0.032	0.000
28	0.063	0.002	0.002	0.055	0.046	-0.001
31	0.092	0.004	0.003	0.082	0.085	0.003
34	0.112	0.002	0.000	0.112	0.106	0.002
37	0.141	0.001	0.004	0.144	0.143	0.001
40	0.175	0.004	0.002	0.165	0.177	0.002
43	0.202	0.006	0.003	0.192	0.202	0.003

Table 5
Thermal test results of dial indicator 1 and dial indicator 3.

T (℃)	The average value of dial indicator 1 (mm)	The average value of dial indicator 3 (mm)
25	0.032	0.032
28	0.065	0.064
31	0.101	0.103
34	0.147	0.144
37	0.182	0.182
40	0.225	0.226
43	0.253	0.244

$$\Delta L_{CY} = \left(\lambda - \left(1 + a \triangle T\right)\sqrt{\lambda^2 + \eta^2}\,\sin\left(\arctan\left(\frac{\eta\sigma(\mu-\lambda) + \lambda[1+\sigma+(\mu-\lambda)^2]}{\eta[1+\sigma+(\mu-\lambda)^2] - \lambda\sigma(\mu-\lambda)}\right)\right)\right)L \tag{12}$$

Among them, ΔL_{BX} is the change in the x-direction of point B. ΔL_{CY} is the change in the y-direction of point C. The value of λ and μ is 1, and the value of η is 0.5, and the value of L is 500 mm. The BC two points have a common theoretical thermal displacement formula:

$$\Delta L = \Delta L_{BX} = \Delta L_{CY} = 0.0118t - 0.2596 \tag{13}$$

The data of the dial indicator 1 and dial indicator 3 of the test measurements are proposed, so by the least-squares, we get the fitting equation ΔL_{bx} and ΔL_{cy} of the linear equation of B and C. Expressions are:

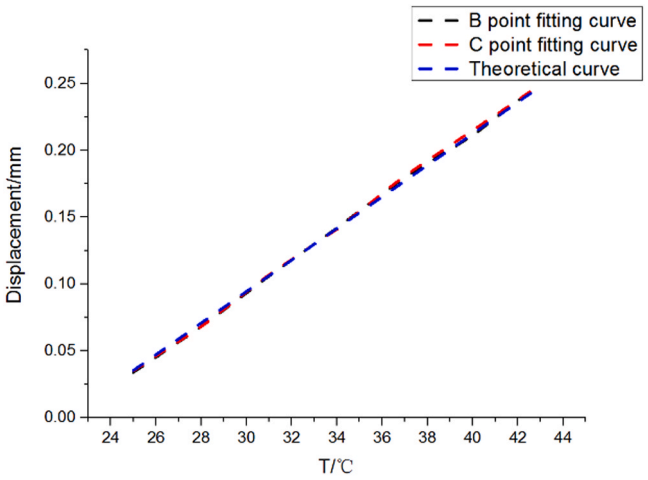

Fig. 12. Temperature-displacement curve.

$$\Delta L_{bx} = 0.0122t - 0.2731 \tag{14}$$

$$\Delta L_{cy} = 0.0121t - 0.2699 \tag{15}$$

The fitting results are compared with the theoretical formula as follows:

$$\begin{cases} \delta_1 = \dfrac{\Delta k_B}{k} = \dfrac{0.0122 - 0.0118}{0.0118} = 3.4\% \\ \delta_2 = \dfrac{\Delta k_C}{k} = \dfrac{0.0121 - 0.0118}{0.0118} = 2.5\% \\ \delta_3 = \dfrac{\Delta b_B}{b} = \dfrac{0.2731 - 0.2596}{0.2596} = 5.3\% \\ \delta_4 = \dfrac{\Delta b_C}{b} = \dfrac{0.2699 - 0.2596}{0.2596} = 3.9\% \end{cases} \tag{16}$$

Among them, δ_1 is the slope of the slope relative to the slope of the temperature of B in the x-direction, which is 3.4%. δ_2 is the slope of the slope relative to the slope of the temperature of C in the y-direction, which is 2.5%. δ_3 is 5.3%the rate of the intercept relative to the relative theoretical intercept of B in the x-direction temperature rise test. δ_4 is 3.9% of the intercept relative to the relative theoretical intercept of C point in the y-direction. As shown in Fig. 12, the experimental data show that the test value and the theoretical error rate are less than 6%, indicating that the interface mechanism can release the thermal stress well and ensure the stability of the back-end module of the space telescope.

After heating, waiting for the temperature to drop naturally and the temperature to return to room temperature, the position of the four target balls measured by the laser tracker is similar to that before the temperature change, which proves that the interface has good reset. That is, the interface can maintain high consistency in both space heating and non-working space variation.

4. Conclusion

In this paper, the influence of temperature change on the location of an interface mechanism is studied. When the space telescope is in orbit, it is affected by the violent temperature change, which affects the position of the location point and the relative change of the location point in the interface mechanism, which directly determines the imaging quality of the space telescope. The following conclusions are drawn:

1. Based on the kinematics principle of 3-2-1, the mathematical expression of the positioning accuracy of the back-end module between the temperature change and the interface layout is derived. The positioning variation of BC two points and the centroid E is obtained. The results show that when the connection of the AB two points coincides with the positioning axis of the B point, the inner rotation angle of the back-end module is the smallest in the A, B, C three points.
2. Through the relationship between the four independent variables *λ, μ, η, t and the change of the central point* ΔE, it is concluded that when A, B, C three-point layout is obtained, to make the back-end module have the highest stability, the order of variable design should be *η, t,* λ *and* μ. *When* η *and t values are determined, for the highest stability of the module,* λ *and* μ *must have a linear relationship, and different* η *and t determine different linear scaling factors, when* η *values 0.5, t to 30, the back-end module wants to make the maximum stability, which must make the* $\mu = 0.65\lambda$.
3. Verified by the test, the change rate of the slope of interface B's temperature rise test in x-direction relative to the theoretical formula is 3.4%. The change rate of the slope of interface C's temperature rise test in y-direction relative to the theoretical slope is 2.5%. The change rate of the intercept of interface B's temperature rise test in x-direction relative to the theoretical intercept is 5.3%. The change rate of temperature rise test intercept of interface C in y-direction relative to the theoretical intercept is 3.9%. The test data show that the error rate between the experimental value and the theoretical value is less than 6%, which indicates that the interface mechanism can release the thermal stress well and ensure the stability of the back-end module of the space telescope.

Declaration of Competing Interest

We declare that we have no financial and personal relationships with other people or organizations that can inappropriately influence our work, there is no professional or other personal interest of any nature or kind in any product, service and/or company that could be construed as influencing the position presented in, or the review of, the manuscript entitled.

References

[1] J.R.R.E. PACE, Repair of Major System Elements on Skylab, 1974.
[2] J. VON Puttkamer, Skylab: Its Anguish and Triumph-A Memoir, 1982.
[3] N.E. Brown, E.L. Saenger. EVA Crew Workstation Provisions for Skylab and Space Shuttle missions, 1973.
[4] W.D. Compton, C.D. Benson, Proteolytic fragmentation of rat prolactin by the rat ventral prostate gland, Prostate 4 (1983) 231–246.
[5] D. Hitt, O.K. Garriott, J. Kerwin, Homesteading Space: the Skylab Story, U of Nebraska Press, 2008.
[6] J.D. Bohlin, K.J. Frost, P.T. Burr, A.K. Guha, G.L. Withbroe, Solar maximum mission, Sol. Phys. 65 (1) (1980) 5–14.
[7] Y. Ogawara, T. Takano, T. Kato, T. Kosugi, S. Tsuneta, T. Watanabe, I. Kondo, Y. Uchida, The solar-a mission: an overview, The Yohkoh (Solar-A) Mission, 1991, pp. 1–16.

[8] B.E. Woodgate, S.P. Maran, The solar maximum mission repair-lessons learned, in: Proceedings of the Space Station Automation II, F, International Society for Optics and Photonics, 1987.
[9] R.J. Hedgeland, P.A. Hansen, D.W. Hughes, Integrated approach for contamination control and verification for the Hubble Space Telescope first servicing mission, Proc. SPIE- Int. Soc. Opt. Eng. (1994) 10–21.
[10] T.E. Styczynski, Hubble space telescope first servicing mission, SAE Trans. (1994), 942123.
[11] P.A. Hansen, D.W. Hughes, J.J. Triolo, et al., Hubble Space Telescope second servicing mission contamination control program, Proc. SPIE- Int. Soc. Opt. Eng. (1996) 27–35.
[12] E. Cheng, L. Feinberg, P. Geithner, D. Scheve, L. Abramowicz-Reed, Second HST servicing mission: expanding the new frontier, Opt. Photonics News 8 (1) (1997) 23.
[13] R. Phillips, Hubble Space Telescope Second Servicing Mission Extra Vehicular Activity Report. Lockheed Martin Missiles and Space, Sunnyvale, CA, 1999.
[14] J. Grunsfeld, S. Altman, D. Carey, et al., Hubble Space Telescope fourth servicing mission: the perspective from orbit, Bull. Am. Astron. Soc. (2002).
[15] J.M. Grunsfeld, C.M. Foale, C. Nicollier, et al., Hubble Space Telescope Third Servicing Mission: The Perspective from Orbit, 1999.
[16] D. Fischer, H. Duerbeck, Hubble's Next Decade. Hubble, Springer, 1996, pp. 160–163.
[17] R.A. Kimble, J.W. Mackenty, R.W. O'Connell, et al., Wide Field Camera 3: a powerful new imager for the Hubble Space Telescope, Proc. SPIE- Int. Soc. Opt. Eng. 7010 (2008), 70101E-70101E-12.
[18] D.E. Hastings, C. Joppin, On-orbit upgrade and repair: the Hubble space telescope example, J. Spacecr. Rockets 43 (3) (2006) 14–25, 6.
[19] I. KAWANO, Space vehicle guidance and control using GPS: autonomous rendezvous docking of ETS-VII, J. Soc. Instrum. Control Eng. (2005) 44.
[20] M. Oda, T. Inagaki, M. Nishida, et al., Design and development status of ETS-7, an RVD and space robot experiment satellite, in: Proceedings of the Artificial Intelligence, Robotics, and Automation for Space Symposium, 1994.
[21] I. Kawano, M. Mokuno, T. Kasai, et al., Result and evaluation of autonomous rendezvous docking experiment of ETS-VII, in: Proceedings of the Guidance, Navigation, & Control Conference & Exhibit, 2013.
[22] M. Nohmi, K. Matsumoto, H. Ueno, et al., Deployable truss operation by ETS-VII robot arm using force accommodation control, Comput. -Aided Civ. Infrastruct. Eng. (2010) 16.
[23] M.A. Greenhouse, P.C. Sullivan, L.A. Boyce, S.D. Glazer, E.L. Johnson, J.C. McCloskey, M.F. Voyton, The James Webb Space Telescope integrated science instrument module, Proc. SPIE 754–764 (2004), 754.
[24] Brent J. Bos, Joseph M. Howard, Philip J. Young, Renee Gracey, Lenward T. Seals, Raymond G. Ohl, Global alignment optimization strategies, procedures, and tools for the James Webb Space Telescope (JWST) Integrated Science Instrument Module (ISIM), Proc. SPIE 8442, Space Telescopes and Instrumentation: Optical, Infrared, and Millimeter Wave, 84423I (2012/09/21), 2012.
[25] G.S. Wright, G.H. Rieke, L. Colina, E. van Dishoeck, G. Goodson, T. Greene, P.O. Lagage, A. Karnik, S.D. Lambros, D. Lemke, M. Meixner, H.U. Norgaard, G. Oloffson, T. Ray, M. Ressler, C. Waelkens, D. Wright, A. Zhender, The JWST MIRI instrument concept, Proc. SPIE 653–663 (2004), 653.
[26] N. Rowlands, D. Aldridge, R. Allen, C. Evans, P. Gregory, E. Hartwig, B. Mackay, J. Metcalfe, G. Richardson, D. Caldwell, R. Deschambault, T. Girard, J. Hackett, D. Henry, J.B. Hutchings, C. Morbey, R. Murowinski, R. Doyon, R. Alexander, The JWST fine guidance sensor, Proc. SPIE 664–675 (2004), 664.
[27] N. Rowlands, C. Evans, E. Greenberg, P. Gregory, A. Scott, S. Thibault, M. Poirer, R. Doyon, J. Hutchings, R. Alexander, Tunable filters for JWST fine guidance sensor, Proc. SPIE 676–687 (2004), 676.
[28] B.J. Bos, D.A. Kubalak, S.R. Antonille, R.G. Ohl, J.G. Hagopian, P.S. Davila, J. Sullivan, M. Sánchez, Cryogenic pupil alignment test architecture for the James Webb Space Telescope integrated science instrument module, Proc. SPIE (2008), 70103C.
[29] F.G. Wang, Study on the influence of temperature and support style to the 1.2 m Sic primary mirror surface figure, Acta Photonica Sin. 40 (06) (2011) 933–936.
[30] L. Kong, L. Yang, Study and test of thermal-defocusing property in space camera, Opt. Precis. Eng. 25 (07) (2017) 1825–1831.
[31] H.B. Liu, J.C. Tan, B.J. Shen, Thermal/structural/optical analysis of optical system of star sensor, J. Astronaut. 31 (03) (2010) 875–879.
[32] X. Yang, S.Y. Xu, X.B. Li, et al., Influences of temperature gradient on thermal stability tolerance of large aperture reflective mirror, Infrared Laser Eng. 48 (09) (2019) 207–216.
[33] Y. Yuan, L.H. Chen, L.B. Yang, et al., Precision of kinematic coupling mechanism for optical instruments, Optik (2019), 163592.
[34] Q.Y. Li, W.G. Zhao, Z. Shi, et al., Research on positioning mechanism of optical device based on-orbit replacement, Opt. Precis. Eng. 27 (10) (2019) 2233–2240.
[35] Z. Shi, W.G. Zhao, Q.Y. Li, et al., Research on interface mechanism of back-end module for on-orbit maintenance, Opt. Precis. Eng. 28 (3) (2020) 649–658.